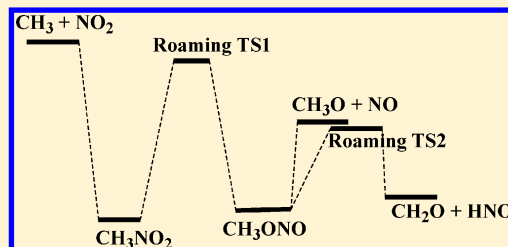


Effect of Roaming Transition States upon Product Branching in the Thermal Decomposition of CH_3NO_2 R. S. Zhu,[†] P. Raghunath,[‡] and M. C. Lin^{*,†,‡}[†]Department of Chemistry, Emory University, Atlanta, Georgia 30322, United States[‡]Center for Interdisciplinary Molecular Science, Department of Chemistry, National Chiao Tung University, Hsinchu, Taiwan 300

S Supporting Information

ABSTRACT: The kinetics for the thermal unimolecular decomposition of CH_3NO_2 and its structural isomer CH_3ONO have been investigated by statistical theory calculations based on the potential energy surface calculated at the UCCSD(T)/CBS and CASPT3(8, 8)/6-311+G(3df,2p) levels. Our results show that for the decomposition of CH_3NO_2 at pressures less than 2 Torr, isomerization to CH_3ONO via the recently located roaming transition state is dominant in the entire temperature range studied, 400–3000 K. However, at higher pressures, the formation of the commonly assumed products, $\text{CH}_3 + \text{NO}_2$, becomes competitive and at pressures higher than 200 Torr the production of $\text{CH}_3 + \text{NO}_2$ is exclusive. The predicted rate constants for 760 Torr and the high-pressure limit with Ar as diluent in the temperature range 500–3000 K, producing solely $\text{CH}_3 + \text{NO}_2$, can be expressed respectively by $k_d^{760}(\text{CH}_3\text{NO}_2) = 2.94 \times 10^{55} T^{-12.6} \exp(-35500/T) \text{ s}^{-1}$ and $k_d^\infty(\text{CH}_3\text{NO}_2) = 5.88 \times 10^{24} T^{-2.35} \exp(-31400/T) \text{ s}^{-1}$. In the low pressure limit, the decomposition reaction takes place exclusively via the roaming TS producing internally excited CH_3ONO , giving rise to both $\text{CH}_3\text{O} + \text{NO}$ and $\text{CH}_2\text{O} + \text{HNO}$ with the second-order rate constant $k_d^0(\text{CH}_3\text{NO}_2) = 1.17 \times 10^{31} T^{-10.94} \exp(-32400/T) \text{ cm}^3 \text{ molecule}^{-1} \text{ s}^{-1}$. For CH_3ONO decomposition, a new roaming transition state connecting to the $\text{CH}_2\text{O} + \text{HNO}$ products has been located, lying 6.8 kcal/mol below the well-known four-member ring tight transition state and 0.7 kcal/mol below $\text{CH}_3\text{O} + \text{NO}$. The rate constants predicted by similar calculations give rise to the following expressions for the thermal decomposition of CH_3ONO in He: $k_d^{760}(\text{CH}_3\text{ONO}) = 8.75 \times 10^{41} T^{-8.97} \exp(-22600/T) \text{ s}^{-1}$ and $k_d^\infty(\text{CH}_3\text{ONO}) = 1.58 \times 10^{23} T^{-2.18} \exp(-21100/T) \text{ s}^{-1}$ in the temperature range 300–3000 K. These results are in very good agreement with available experimental data obtained under practical pressure conditions. The much different branching ratios for the formation of $\text{CH}_3\text{O} + \text{NO}$ and $\text{CH}_2\text{O} + \text{HNO}$ in the decomposition of both CH_3NO_2 and CH_3ONO are also given in this work.



1. INTRODUCTION

The thermal decomposition of CH_3NO_2 , a prototype energetic material that contains the key [C,H,O,N] ingredients of nitro and nitro-amine compounds, is relevant not only to the combustion of energetic materials but also to its related recombination reaction $\text{CH}_3 + \text{NO}_2$, which is relevant to the pollution chemistry in the troposphere. There have been many studies on the kinetics and mechanism of the unimolecular decomposition reaction of CH_3NO_2 and the related $\text{CH}_3 + \text{NO}_2$ reaction.¹ The results of some of the key measurements will be cited for comparison with the predicted values later. To date, the thermal decomposition of CH_3NO_2 has been nearly exclusively assumed to take place by C–N splitting:



Other potential decomposition channels via the well-known nitro-nitrite isomerization and the H-atom migration and dehydration processes producing HCNO via $\text{CH}_2=\text{N}(\text{O})\text{OH}$ all occur by tighter and energetically less favorable transition states^{2–6} and thus cannot compete with the C–N breaking process with 60 kcal/mol dissociation energy aided by its loose transition state without an intrinsic barrier.

In 1986, an interesting result on the detection of $\text{CH}_3\text{O} + \text{NO}$ was reported by Wodtke, Hinstä, and Lee⁷ in their IRMPD (infrared multiphoton decomposition) of CH_3NO_2 under a collision-free molecular beam condition using a high-power CO_2 laser. This observation could not be satisfactorily accounted for theoretically for nearly a quarter of a century with reliable computational methods based on the nitro-nitrite isomerization mechanism because the process is both entropically unfavorable and enthalpically inaccessible in the IRMPD experiment.^{3–6}

In 2004, a new mechanism for molecular decomposition, termed “roaming mechanism” was first discovered by a joint experimental–theoretical study on the photodissociation of H_2CO .⁸ On the basis of the systems studied in the last several years,^{9–12} roaming transition states (RTS) are typically found to locate at the radical–radical separations of about 3–4 Å, where the radicals may sample orientations leading to

Special Issue: Joel M. Bowman Festschrift

Received: January 31, 2013

Revised: June 10, 2013

Published: June 13, 2013

intramolecular abstractions with barriers around 1–2 kcal/mol below the lowest bond cleavage paths. The implication of this finding to the initiation mechanisms of combustion and explosion of energetic materials is profound because the thermal decomposition of energetic materials typically occurs via the lowest energy paths with favorable entropic changes.

In 2009, motivated by the roaming mechanism as aforementioned, we attempted to search for and successfully located a very loose roaming type transition state for the isomerization of CH_3NO_2 to CH_3ONO using different computational methods.¹³ The existence of the RTS below the $\text{CH}_3 + \text{NO}_2$ dissociation limit allowed us to reasonably explain the experimental observation cited above by Wodtke, Hinsta, and Lee⁷ in their IRMPD of CH_3NO_2 with as much as 40% CH_3O yield.

On the grounds that the thermal decomposition process occurs energetically close to that of IRMPD, the initial formation of $\text{CH}_3\text{O} + \text{NO}$ and potentially $\text{CH}_2\text{O} + \text{HNO}$ in the thermal unimolecular decomposition of CH_3NO_2 may be competitive with the commonly assumed $\text{CH}_3 + \text{NO}_2$ product formation. In this work, we have accordingly investigated computationally the kinetics for the thermal decomposition of CH_3NO_2 on the basis of the potential energy surface (PES) reported previously¹³ employing the variational RRKM theory to predict the formation of the three key product pairs $\text{CH}_3 + \text{NO}_2$, $\text{CH}_3\text{O} + \text{NO}$, and $\text{CH}_2\text{O} + \text{HNO}$ as functions of temperature and pressure; these results may be helpful for simulations of the decomposition and combustion of CH_3NO_2 , CH_3ONO and larger nitro- and nitramine compounds.

2. COMPUTATIONAL METHODS

The computational approach for the mapping of PES including our extensive search for the roaming transition state (RTS1) and the calculation of the microcanonical rate constants for the fragmentation of excited CH_3NO_2 and CH_3ONO as functions of energy have been described in detail previously (Figure 1).¹³

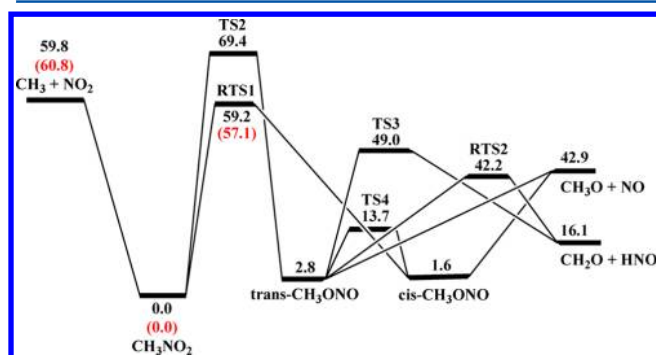


Figure 1. Energy diagrams (in kcal/mol. at 0 K) for the CH_3NO_2 decomposition, computed at the UCCSD(T)/CBS level. The values for CH_3NO_2 and RTS1 in the parentheses were calculated at the CASPT3(8,8)/6-311+G(3df,2p)//CASCF(8,8)/6-311+G(d) level.

For the decomposition of CH_3ONO , another roaming transition state (RTS2) for the production of $\text{CH}_2\text{O} + \text{HNO}$ has been located in this work; it is distinctively different from the well-known four-center tight transition state (TS3). In RTS2 the dissociating NO group roams around the CH_3O fragment and abstracts one of the H atoms from the CH_3 group to yield $\text{CH}_2\text{O} + \text{HNO}$ (see SI-3, Supporting Information). The rate constants were computed with a variational RRKM code (Variflex¹⁴) by solving the master equation^{15,16} involving

multistep vibrational energy transfers for the excited intermediate CH_3NO_2^* or CH_3ONO^* based on the PES calculated at the UCCSD(T)/CBS//UB3LYP/6-311+G(3df,2p) and CASPT3(8,8)/6-311+G(3df,2p) levels of theory, as shown in Figure 1.

The energies used in the rate constant calculations are mainly based on the UCCSD(T)/CBS//UB3LYP/6-311+G(3df,2p) level; among them, the energy of the loose RTS1 obtained at the CASPT3(8,8)/6-311+G(3df,2p) level was used, similar to those of the variational transition states (VTS's) for bond breaking processes described below. Frequencies and rotational constants used in the calculations are taken from the UB3LYP/6-311+G(3df,2p) level. The Cartesian coordinates of the related species are listed in Supporting Information (SI-1). The variational dissociation curve for $\text{CH}_3\text{NO}_2 \rightarrow \text{CH}_3 + \text{NO}_2$ was calculated at the CASPT2(8,8)/6-311+G(3df,2p)//UB3LYP/6-311+G(3df,2p) level to cover the C–N bond with separation from 1.499 to 4.699 Å, with an interval step size of 0.2 Å, other geometric parameters were fully optimized. The dissociation curve can be fitted to the Morse potential function $E(R) = D_e[1 - \exp(-\beta(R - R_e))]^2$, which was employed to approximate the minimum energy path for the variational transition state of $\text{CH}_3\text{NO}_2 \rightarrow \text{CH}_3 + \text{NO}_2$. In the above equation, R is the reaction coordinate (i.e., the distance between the two bonding atoms; the C–N in this work), D_e is the bond energy excluding zero-point energy, and R_e is the equilibrium value of R . The computed potential energies could be fitted reasonably to the Morse potential function with the parameter $\beta = 2.223 \text{ \AA}^{-1}$ (see SI-2, Supporting Information). The barrierless dissociation of CH_3ONO to $\text{CH}_3\text{O} + \text{NO}$ was calculated similarly with $\beta = 2.552 \text{ \AA}^{-1}$. For both barrierless processes, the number of a variational transition quantum states, N_{EJ}^{\dagger} , was given by the variationally determined minimum in $N_{\text{EJ}}(R)$, as a function of the bond length along the reaction coordinate R , which was evaluated according to the variable reaction coordinate flexible transition state theory.^{17,18} The estimation of the transitional mode contribution to the transition state number of states for a given energy is evaluated via Monte Carlo integration with 10 000 configuration numbers. The numbers of states for RTS1 and RTS2 are evaluated according to the rigid-rotor harmonic-oscillator assumption, the smaller frequencies (less than 50 cm^{-1}) were treated as a free or hindered rotor.

For the collisional energy transfer calculations, the L-J parameters required for the RRKM calculations for the quenching of $\text{CH}_3\text{NO}_2/\text{CH}_3\text{ONO}$ are taken from ref 19, $\epsilon/k = 290.4 \text{ K}$ and $\sigma = 4.347 \text{ \AA}$, and those for He and Ar, $\epsilon/k = 10$ and 114 K and $\sigma = 2.55$ and 3.47 \AA , respectively, were taken from the literature.²⁰ The energy–transfer process was computed on the basis of the exponential down model with a $\langle \Delta E \rangle_{\text{down}}$ value (the mean energy transferred per collision) of 150 and 400 cm^{-1} for He and Ar, respectively.

3. RESULTS AND DISCUSSION

3.1. Rate Constants for the Decomposition of CH_3NO_2 . On the basis of the PES summarized in Figure 1, the thermal decomposition of CH_3NO_2 may take place preferentially by the following three low-energy paths:



The bond-breaking processes in reactions 1 and 2 occur by variational transition states that were computed at the CASPT2(8,8)/6-311+G(3df,2p)//UB3LYP/6-311+G(3df,2p) level of theory as aforementioned, whereas the first step in reaction 2 is mainly controlled by RTS1 in Figure 1. For reaction 3, as aforementioned, we have located a new roaming transition state, RTS2, lying 0.7 kcal/mol below $\text{CH}_3\text{O} + \text{NO}$ predicted at the CCSD(T)/CBS//UB3LYP/6-311+G(3df,2p) level. It should be noted that the possibility of existence of the loose TS similar to RTS1 in the nitro–nitrite isomerization reaction had also been reported by Mckee⁴ in 1989 for the CH_3NO_2 isomerization process using the CAS(4,4)/6-31G(d) method; however, the loose TS was found to lie 10.0 kcal/mol above the $\text{CH}_3 + \text{NO}_2$ limit at the MRCI/6-31G(d)//CAS/6-31G(d) level. Subsequently, Saxon and Yoshimine⁶ had also located a loose TS at the MRCI(7,7)/6-31G(d)//CAS(4,4)/4-31G level of theory; their TS was found to lie 56.7 kcal/mol above CH_3NO_2 and 0.4 kcal/mol below the $\text{CH}_3 + \text{NO}_2$ asymptote, energetically akin to our RTS1 value computed at the CASPT2 level of theory. The well-known nitro–nitrite isomerization path occurring via TS2, however, lies above the $\text{CH}_3 + \text{NO}_2$ dissociation limit by 9.6 kcal/mol, which is consistent with the results of previous calculations.^{3–6} The contribution from this path should therefore be kinetically negligible.

Experimentally, most of the CH_3NO_2 decomposition rates were measured in the pressure range 150–30400 Torr Ar,^{21–29} the reported main products are $\text{CH}_3 + \text{NO}_2$. Due to the location of the RTS1 below the $\text{CH}_3 + \text{NO}_2$ dissociation limit, CH_3NO_2 can isomerize to *cis*- CH_3ONO , which further decomposes to give $\text{CH}_3\text{O} + \text{NO}$ and $\text{CH}_2\text{O} + \text{HNO}$, as shown in Figure 1. Figure 2 shows the pressure dependent rate constants predicted at 1000 and 1500 K for the two competing reactions 1 and 2 in the pressure range 10^{-5} to 760 Torr Ar. At both temperatures, the decomposition is found to be dominated by the production of CH_3ONO via RTS1 below about 2 Torr pressure, above which the formation of $\text{CH}_3 +$

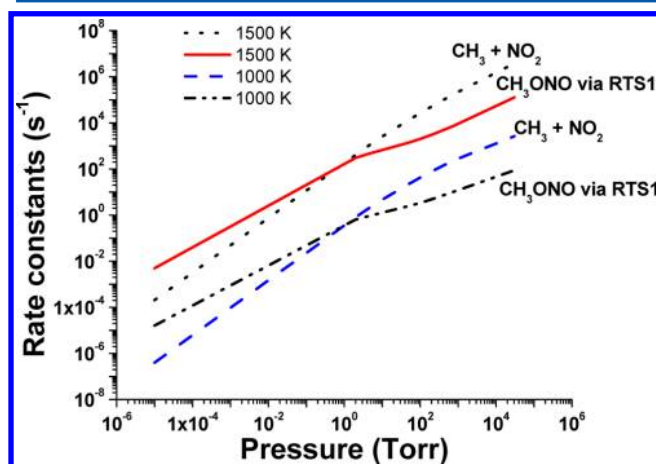


Figure 2. Predicted rate constants for the formation of $\text{CH}_3 + \text{NO}_2$ and CH_3ONO via RTS1 in the decomposition of CH_3NO_2 at 1000 and 1500 K under different pressures.

NO_2 becomes competitive and dominant at $P > 200$ Torr. Figure 3 presents the branching ratios for CH_3ONO formation

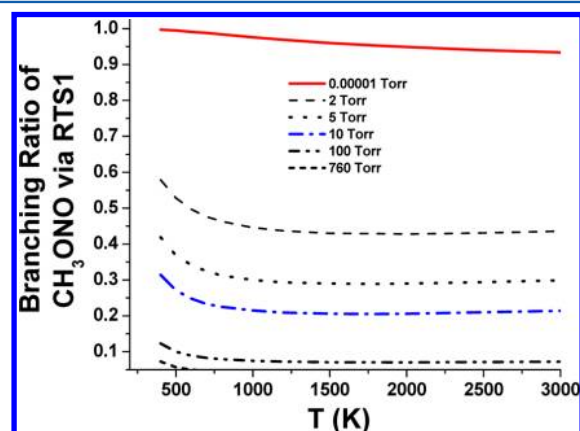


Figure 3. Predicted branching ratios for the formation of CH_3ONO via RTS1 at pressures between 10^{-5} and 760 Torr for the decomposition of CH_3NO_2 in the temperature range 400–3000 K.

via RTS1 in the decomposition of CH_3NO_2 at various pressures in the temperature range 400–3000 K. The results most vividly illustrate the competition between the two decomposition reactions; at pressures lower than 2 Torr, isomerization of CH_3NO_2 to CH_3ONO via RTS1 is dominant in the whole temperature range, whereas at $P > 200$ Torr, more than 90% of the products are $\text{CH}_3 + \text{NO}_2$. Our results can thus explain why most of the investigators did not observe the $\text{CH}_3\text{O} + \text{NO}$ products under practical, higher pressure conditions.

The calculated first-order rate constants for the decomposition of CH_3NO_2 are plotted in Figure 4 for comparison

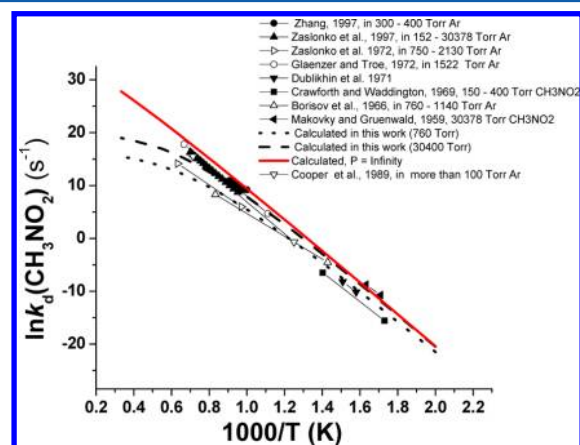


Figure 4. Comparison of the predicted first-order rate constant for CH_3NO_2 decomposition with experimental values in Ar. Dotted, dashed, and solid lines are the predicted values at 760 and 30400 Torr Ar and infinite pressure. Symbols in the legend are the experimental values.

with available literature data. Calculated values at 760 and 30400 Torr Ar and at the high-pressure limit are plotted as dotted, dashed, and solid lines in the figure, indicating that, under most experimental conditions, our predicted values lie within the scatter of experimental data.

The rate constants for 760 Torr and the high-pressure limit with Ar dilution in the temperature range 500–3000 K,

representing the values for production of $\text{CH}_3 + \text{NO}_2$, can be expressed respectively by

$$k_d^{760}(\text{CH}_3\text{NO}_2) = 2.94 \times 10^{55} T^{-12.6} \exp(-35500/T) \text{ s}^{-1}$$

$$k_d^\infty(\text{CH}_3\text{NO}_2) = 5.88 \times 10^{24} T^{-2.35} \exp(-31400/T) \text{ s}^{-1}$$

The CH_3NO_2 isomerization rate constant in the collision-controlled, second-order, low-pressure limit, which represents exclusively for formation of CH_3ONO , can be given by

$$k_d^0(\text{CH}_3\text{NO}_2) = 1.17 \times 10^{31} T^{-10.94} \exp(-32379/T) \text{ cm}^3 \text{ molecule}^{-1} \text{ s}^{-1}$$

As aforementioned and depicted in Figure 1, the barrier of RTS2 is 6.8 kcal/mol lower than that of TS3, lying below the $\text{CH}_3\text{O} + \text{NO}$ dissociation limit by 0.7 kcal/mol. On the basis of this new RTS2, the calculated rate constants under the conditions of 10^{-5} to 760 Torr Ar and 300–3000 K temperature for $\text{CH}_3\text{NO}_2 \rightarrow \text{CH}_3\text{ONO}^* \rightarrow \text{CH}_3\text{O} + \text{NO}$ (k_2) can be represented as

$$k_2 = 8.91 \times 10^{19} T^{-1.84} \exp(-30600/T) \text{ s}^{-1}$$

and $\text{CH}_3\text{NO}_2 \rightarrow \text{CH}_3\text{ONO}^* \rightarrow \text{CH}_2\text{O} + \text{HNO}$ (k_3) represents as

$$k_3 = 2.15 \times 10^{17} T^{-0.75} \exp(-30200/T) \text{ s}^{-1}$$

The branching ratios of these two channels are shown in Figure 5. Combining Figures 3 and 5, one can see that, at low

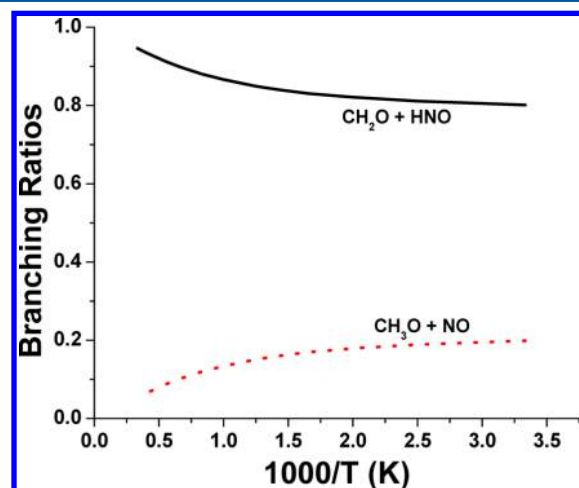


Figure 5. Predicted branching ratios for the formation of $\text{CH}_3\text{O} + \text{NO}$ and $\text{CH}_2\text{O} + \text{HNO}$ in the thermal decomposition of CH_3NO_2 via CH_3ONO at pressure 10^{-5} to 760 Torr Ar.

pressures, the formation of $\text{CH}_2\text{O} + \text{HNO}$ from the fragmentation of internally excited CH_3ONO formed by the isomerization via RTS1 is dominant in the whole temperature range.

3.2. Rate Constants for the Decomposition of CH_3ONO . We have also taken the opportunity to calculate the rate constants for the competitive decomposition of CH_3ONO to $\text{CH}_3\text{O} + \text{NO}$ and $\text{CH}_2\text{O} + \text{HNO}$. The predicted rate constants for the products of $\text{CH}_3\text{O} + \text{NO}$ at 100 and 760 Torr and the high-pressure limit are plotted in Figure 6 for comparison with available literature data. The predicted values are seen to be in good agreement with experimental data measured with different diluents,^{30–37} as shown in the figure,

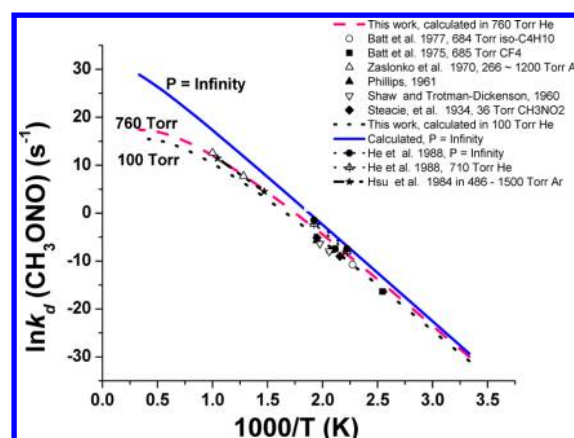


Figure 6. Comparison of the predicted first-order rate constant for the decomposition of $\text{CH}_3\text{ONO} \rightarrow \text{CH}_3\text{O} + \text{NO}$ with the experimental values in He. Dotted, dashed and solid lines are the predicted values at 100 and 760 Torr He and infinite pressure. Symbols in the legend are the experimental data.

including He for which the rate constants measured at 710 Torr pressure with the extrapolated high pressure limit have been reported.³⁰ The predicted results for 760 Torr He and the high- and low-pressure limits in the temperature range 300–3000 K can be expressed respectively by

$$k_d^{760}(\text{CH}_3\text{ONO}) = 8.75 \times 10^{41} T^{-8.97} \exp(-22600/T) \text{ s}^{-1}$$

$$k_d^\infty(\text{CH}_3\text{ONO}) = 1.58 \times 10^{23} T^{-2.18} \exp(-21100/T) \text{ s}^{-1}$$

$$k_d^0(\text{CH}_3\text{ONO}; \text{He}) = 8.91 \times 10^{19} T^{-7.92} \exp(-22300/T) \text{ cm}^3 \text{ molecule}^{-1} \text{ s}^{-1}$$

On the basis of RTS2, the branching ratios for the production of $\text{CH}_2\text{O} + \text{HNO}$ and $\text{CH}_3\text{O} + \text{NO}$ have been calculated and shown in Figure 7 as a function of temperature at 10^{-5} and 760 Torr Ar pressure. The results show that at low temperatures and low pressures, the main products are $\text{CH}_2\text{O} + \text{HNO}$; however, at $P = 1$ atm, two channels are very

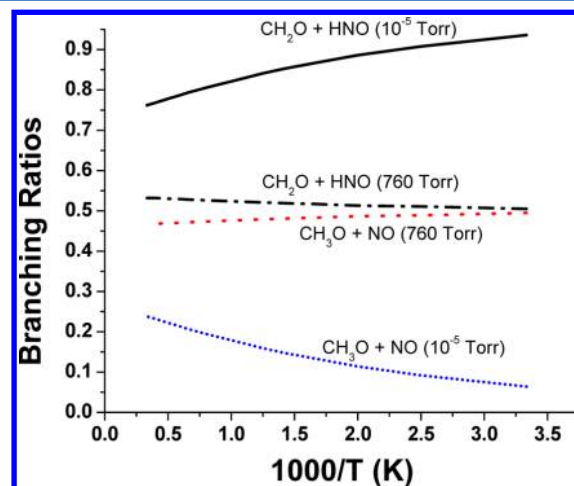


Figure 7. Predicted branching ratios for the formation of $\text{CH}_3\text{O} + \text{NO}$ and $\text{CH}_2\text{O} + \text{HNO}$ in the thermal decomposition of CH_3ONO at pressure 10^{-5} and 760 Torr Ar.

competitive. It is worth noting that the branching ratios predicted for the formation of CH_3NO_2 (Figure 5) and those in the thermal decomposition of CH_3ONO (Figure 7) are distinctively different. The former values are pressure-independent between 10^{-5} and 760 Torr, reflecting the fragmentation of highly excited CH_3ONO with 57.1 kcal/mol of internal energy via RTS1 (akin to a chemical activation process), whereas the latter values reflect the collisional activation of CH_3ONO from the ground up as in a typical thermal unimolecular decomposition reaction.

Due to the very flat potential energy surfaces around the roaming transition states RTS1 and RTS2, accurate determination of relative contributions to the dissociation products from these roaming channels versus the conventional product channels needs extensive trajectory simulations based on a complete potential surface which is beyond the scope of this work.

4. CONCLUSION

In this study, the kinetics for the thermal unimolecular decomposition of CH_3NO_2 and its structural isomer CH_3ONO have been calculated by variational RRKM theory based on the PES recently computed by two of the present authors at the UCCSD(T)/CBS//UB3LYP/6-311+G(3df,2p) and CASPT3(8,8)/6-311+G(3df,2p) levels of theory.¹³ As alluded to in the Introduction, the location of a loose roaming type transition state for the isomerization of CH_3NO_2 to CH_3ONO allowed us to fully account for the production of CH_3O with as much as 40% yield by IRMPD under the collision-free molecular beam condition reported by Wodtke et al.⁷ The results of the present study based on the PES shows that under the thermal condition, which is similar to that of IRMPD, the isomerization production of CH_3ONO is dominant at pressures below 2 Torr in the temperature range studied, 400–3000 K, whereas the formation of the $\text{CH}_3 + \text{NO}_2$ products becomes competitive at pressures higher than 2 Torr. At 200 Torr pressure, for example, the production of the latter product pairs accounts for more than 90% of the decomposition reaction. Accordingly, the predicted high-pressure limit rate constant represents solely for the production of $\text{CH}_3 + \text{NO}_2$, whereas the predicted second-order, low-pressure limit rate constant represents entirely for the formation of the CH_3ONO , which further decomposes competitively to $\text{CH}_3\text{O} + \text{NO}$ and $\text{CH}_2\text{O} + \text{HNO}$ via another roaming transition state.

■ ASSOCIATED CONTENT

Supporting Information

Cartesian coordinates of the main species related to the decomposition of CH_3NO_2 (SI-1), calculated and fitted VTS curve for CH_3NO_2 decomposition (SI-2), and the structure of the roaming transition state RTS2 connecting to $\text{CH}_2\text{O} + \text{HNO}$ (SI-3). This material is available free of charge via the Internet at <http://pubs.acs.org>.

■ AUTHOR INFORMATION

Corresponding Author

*E-mail: chemmcl@emory.edu.

Notes

The authors declare no competing financial interest.

■ ACKNOWLEDGMENTS

The authors acknowledge a partial support from the U.S. Office of Naval Research under contract No. N00014-08-1-0106. M.C.L. also thanks Taiwan's National Science Council for the award of a distinguished visiting professorship at the National Chiao Tung University, Hsinchu, Taiwan, as well as the support from the Ministry of Education under its ATU Program.

■ REFERENCES

- (1) Manion, J. A.; Huie, R. E.; Levin, R. D.; Burgess, D. R., Jr.; Orkin, V. L.; Tsang, W.; McGivern, W. S.; Hudgens, J. W.; Knyazev, V. D.; Atkinson, D. B.; Chai, E.; Tereza, A. M.; Lin, C.-Y.; Allison, T. C.; Mallard, W. G.; Westley, F.; Herron, J. T.; Hampson, R. F.; Frizzell, D. H. *NIST Chemical Kinetics Database, NIST Standard Reference Database 17*, Data version 2008.12, Version 7.0 (Web Version), Release 1.4.3; National Institute of Standards and Technology, Gaithersburg, MD, 20899-8320; Web address <http://kinetics.nist.gov/>.
- (2) Dewar, M. J. S.; Ritchie, J. P.; Alster, J. Ground States of Molecules. 65. Thermolysis of Molecules Containing NO_2 Groups. *J. Org. Chem.* **1985**, *50*, 1031–1036.
- (3) Mckee, M. L. *Ab Initio* Study of Rearrangements on the Nitromethane Potential Energy Surface. *J. Am. Chem. Soc.* **1986**, *108*, 5784–5792.
- (4) Mckee, M. L. MCSCF Study of the Rearrangement of Nitromethane to Methyl Nitrite. *J. Phys. Chem.* **1989**, *93*, 7365–7369.
- (5) Nguyen, M. T.; Le, H. T.; Hajgato, B.; Veszpremi, T.; Lin, M. C. Nitromethane – Methyl Nitrite Rearrangement: A Persistent Discrepancy between Theory and Experiment. *J. Phys. Chem. A* **2003**, *107*, 4286–4291.
- (6) Saxon, R. P.; Yoshimine, M. Theoretical Study of Nitro-Nitrite Rearrangement of CH_3NO_2 . *Can. J. Chem.* **1992**, *70*, 572–579.
- (7) Wodtke, A. M.; Hints, E. J.; Lee, Y. T. Infrared Multiphoton Dissociation of Three Nitroalkanes. *J. Phys. Chem.* **1986**, *90*, 3549–3558.
- (8) Townsend, D.; Lahankar, S. A.; Lee, S. K.; Chambreau, S. D.; Suits, A. G.; Zhang, X.; Rheinecker, J. L.; Harding, L. B.; Bowman, J. M. The Roaming Atom: Straying from the Reaction Path in Formaldehyde Decomposition. *Science* **2004**, *306*, 1158–1161.
- (9) Grubb, M. P.; Warter, M. L.; Suits, A. G.; North, S. W. Evidence of Roaming Dynamics and Multiple Channels for Molecular Elimination in NO_3 Photolysis. *J. Phys. Chem. Lett.* **2010**, *1*, 2455–2458.
- (10) Hause, Michael L.; Herath, Nuradhika; Rongshun, Zhu; Lin, M. C.; Arthur, G. Suits, Roaming-Mediated Isomerization in the Photodissociation of Nitrobenzene. *Nat. Chem.* **2011**, *3*, 932–937.
- (11) Heazlewood, B. R.; Jordan, M. J. T.; Kable, S. H.; Selby, T. M.; Osborn, D. L.; Shepler, B. C.; Braams, B. J.; Bowman, Joel M. Roaming is the Dominant Mechanism for Molecular Products in Acetaldehyde Photodissociation. *Proc. Natl. Acad. Sci. U. S. A.* **2008**, *105*, 12719–12727.
- (12) Sivaramakrishnan, R.; Michael, J. V.; Wagner, A. F.; Dawes, R.; Jasper, A. W.; Harding, L. B.; Georgievskii, Y.; Klippensteina, S. J. Roaming Radicals in the Thermal Decomposition Of Dimethyl Ether: Experiment and Theory. *Combust. Flame* **2011**, *158*, 618–632.
- (13) Zhu, R. S.; Lin, M. C. CH_3NO_2 Decomposition/Isomerization Mechanism and Product Branching Ratios: An *Ab Initio* Chemical Kinetic Study. *Chem. Phys. Lett.* **2009**, *478* (1–3), 11–16.
- (14) Klippenstein, S. J.; Wagner, A. F.; Dunbar, R. C.; Wardlaw, D. M.; Robertson, S. H. *VARIFLEX*, version 1.00; 1999.
- (15) Gilbert, R. G.; Smith, S. C. *Theory of Unimolecular and Recombination Reactions*; Blackwell Scientific: Carlton, Australia, 1990.
- (16) Holbrook, K. A.; Pilling, M. J.; Robertson, S. H. *Unimolecular Reactions*; Wiley: 1996.
- (17) Wardlaw, D. M.; Marcus, R. A. RRKM Reaction Theory for Transition States of any Looseness. *Chem. Phys. Lett.* **1984**, *110*, 230–234.

- (18) Klippenstein, S. J.; Marcus, R. A. Unimolecular Reaction Rate Theory for Highly Flexible Transition States. *J. Phys. Chem.* **1988**, *92*, 5412–5417.
- (19) Van Leeuwen, M. E. Derivation of Stockmayer Potential Parameter for Polar Fluids. *Fluid Phase Equilib.* **1994**, *99*, 1–18.
- (20) Hippler, H.; Troe, J.; Wendelken, H. J. Collisional Deactivation of Vibrationally Highly Excited Polyatomic Molecules. *J. Chem. Phys.* **1983**, *78*, 6709–6715.
- (21) Zaslanko, I. S.; Petrov, Yu. P.; Smirnov, V. N. Thermal Decomposition of Nitromethane in Shock Waves: The Effect of Pressure and Collision Partners. *Kinet. Catal. (Engl. Transl.)* **1997**, *38*, 321–324.
- (22) Zhang, Y. X.; Bauer, S. H. Modeling The Decomposition Of Nitromethane, Induced by Shock Heating. *J. Phys. Chem. B* **1997**, *101*, 8717–8726.
- (23) Zaslanko, I. S.; Kogarko, S. M.; Mozzhukin, E. B.; Petrov, Yu. P. Thermal Decomposition of Nitromethane in Shock Waves. *Kinet. Catal. (Engl. Transl.)* **1972**, *13*, 1001–1005.
- (24) Glaenger, K.; Troe, J. Thermische Zerfallsreaktionen von Nitroverbindungen I: Dissoziation von Nitromethan. *Helv. Chim. Acta* **1972**, *55*, 2884–2893.
- (25) Dublikhin, V. V.; Nazin, G. M.; Manelis, G. B. Thermal Decomposition of Nitromethane. *Bull. Acad. Sci. USSR Div. Chem. Sci. (Engl. Transl.)* **1971**, *20*, 1247–1248.
- (26) Crowth, C. G.; Waddington, D. J. Reactions Of Nitroalkanes In The Gas Phase. Part 1. - Pyrolysis Of Nitromethane. *Trans. Faraday Soc.* **1969**, *65*, 1334–1349.
- (27) Borisov, A. A.; Kogarko, S. M.; Skachkov, G. I. Thermal Decomposition of Nitromethane. *Kinet. Catal.* **1966**, *1*, 521–526.
- (28) Makovsky, A.; Gruenwald, T. B. The Thermal Decomposition of Nitromethane under High Pressure. *Trans. Faraday Soc* **1959**, *55*, 952–958.
- (29) Cooper, S. C.; Lin, C. Y.; Argetsinger, A.; Lin, M. C. Relative Rate of CH_3NO_2 , CH_3ONO and CH_3ONO_2 Formation in the Thermal Reaction of NO_2 with Acetaldehyde and Di-*t*-Butyl Peroxide at Low Temperatures. *J. Energ. Mater.* **1989**, *7*, 55–75.
- (30) He, Y.; Sanders, W. A.; Lin, M. C. Thermal Decomposition of Methyl Nitrite: Kinetic Modeling of Detailed Product Measurements by Gas-Liquid Chromatography and Fourier Transform Infrared Spectroscopy. *J. Phys. Chem.* **1988**, *92*, 5474–5481.
- (31) Batt, L.; Milne, R. T.; McCulloch, R. D. The Gas-Phase Pyrolysis of Alkyl Nitrites. V. Methyl Nitrite. *Int. J. Chem. Kinet.* **1977**, *9*, 567–587.
- (32) Batt, L.; McCulloch, R. D.; Milne, R. T. Thermochemical and Kinetic Studies of Alkyl Nitrites (RONO)-D(RO-NO), The Reactions between RO. and NO, and the Decomposition RO. *Proc. Symp. Chem. Kinet. Data Upper Lower Atmos.* **1975**, 441–461.
- (33) Zaslanko, I. S.; Kogarko, S. M.; Mozzhukin, E. V.; Petrov, Yu. P.; Borisov, A. A. Thermal Decomposition of Methyl Nitrite in Shock Waves. 1. Initial Stage of Decomposition and Mechanism of Chemiluminescence of H_2CO and HNO . *Kinet. Catal. (Engl. Transl.)* **1970**, *11*, 249–255.
- (34) Phillips, L. The Pyrolysis of Methyl Nitrite. *J. Chem. Soc. London* **1961**, 3082–3090.
- (35) Shaw, R.; Trotman-Dickenson, A. F. The Reactions of Methoxyl Radicals with Alkanes. *J. Chem. Soc.* **1960**, 3210–3215.
- (36) Steacie, E. W. R.; Shaw, G. T. The Homogeneous Unimolecular Decomposition of Gaseous Methyl Nitrite. *Proc. R. Soc. London A* **1934**, *146*, 388–395.
- (37) Hsu, D. S. Y.; Burks, G. L.; Beebe, M. D.; Lin, M. C. Thermal Decomposition of Methyl Nitrite in Shock Waves Studied by Laser Probing. *Int. J. Chem. Kinet.* **1984**, *16*, 1139–1150.